

Characterization of Neutron Flux in a Medical Cyclotron for Research Purposes using Gold foils and GATE8.1

Fouad A. Abolaban^{1,2*}, Mohammed A. Alawi¹, Eslam M. Taha^{1,2}, Ezzat Elmoujarkach^{1,4}, Essam M. Banoqitah¹, Abdulsalam M. Alhawsawi^{1,2,3}, Paolo De Maio⁵, Gaetano Lopopolo⁵, Anna Tolomeo⁵, Vincenzo Dimiccoli⁵, Andrew Nisbet⁶

*corresponding author: e-mail: fabolaban@kau.edu.sa - Cellphone: +966503640153

¹ King Abdulaziz University, Faculty of Engineering, Nuclear Engineering Department, P.O. Box 80204, Jeddah 21589, Saudi Arabia

² King Abdulaziz University, Center for Training & Radiation Prevention, P.O. Box 80204, Jeddah 21589, Saudi Arabia

³ School of Nuclear Science and Engineering, Oregon State University, Corvallis, OR, 97333, United States

⁴ Institute of Medical Engineering, Universität zu Lübeck, Lübeck, Germany

⁵ ITEL TELECOMUNICAZIONI SRL, Ruvo di Puglia (BA), Italy, Via Antonio Labriola Z.I. SNC, 70037

⁶ Department of Medical Physics and Biomedical Engineering, University College London, Malet Place Engineering Building, London WC1E 6BT, UK

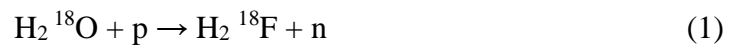
Abstract

The aim of this study is to characterize the neutron flux generated directly behind targets used in medical cyclotrons. The characterization process aims at determining the feasibility of using the generated neutrons for research purposes in Neutron Activation Analysis (NAA). The study was performed by activating gold foils placed directly behind the cyclotron targets. The thermal neutron flux was measured at $1.5\text{E}+06 \pm 5.94\text{E}+04$ (neutrons. cm^{-2} . sec^{-1}). The flux value is the same order of magnitude listed in the manual produced by the cyclotron manufacturer. The results are encouraging and show a high potential for using the cyclotron facility as a thermal column for research purposes. However, it is important radiation protection procedures be followed to ensure the safety of researchers due to the high dose rate measured directly behind the target at 2.46 Sv/ h using an optically stimulated luminescence (OSL) chip during the beam on time.

Keywords: Cyclotron, Characterization, Neutron Activation Analysis, PET trace, Gold foil activation

1. Introduction

Neutrons are produced via several methods such as alpha-induced reaction, neutron-induced fission, spontaneous fission, and from accelerators or cyclotrons as secondary particles [1]. Cyclotrons operate based on the principle of accelerating charged particles that bombard a target to produce both short-lived, long-lived, and proton-rich radionuclides. These radionuclides are supplied to serve a variety of biological, environmental, medical, and industrial applications. Short-lived radionuclides are primarily used in the medical field for both diagnostic and therapeutic procedures in nuclear medicine, including proton emission tomography (PET), computed tomography (CT), and single-photon emission computed tomography (SPECT) [2]. The most common proton emission tomography radiopharmaceutical used in medical cyclotrons is [¹⁸F] fluorodeoxyglucose ([¹⁸F]FDG), which is utilized in tumor imaging and cancer evaluation [3]. To produce ¹⁸F, a beam of protons bombards a target, isolated by a Havar foil, consisting of enriched water (H₂O₁₈). As a result of the beam interaction with the enriched water, fast neutrons are produced from the ¹⁸O (p, n) ¹⁸F reaction [4]. The reaction equation is described as:



In the light of recent developments in facilities housing medical cyclotrons, there have been efforts to characterize neutron flux and energy. The spatial neutron distribution in the vicinity of the cyclotron room has been modeled through Monte Carlo codes and studied experimentally by applying different methods such as gold foil activation (as neutron monitors) and imaging plates [5]–[10]. One of the essential factors in the characterization process is the induced activity of vault materials caused by neutron activation inside the cyclotron vault. To reduce the dose of cyclotron operators, there have been several attempts to measure the activity of the cement composition in the walls, ceiling, and floor of cyclotron rooms. Cyclotrons are designed with different setups based on customer needs. Some are delivered with a self-shield, and some are not. Various researches have examined the activity with and without self-shielding and proposed designs that keep the clearance levels within acceptable limits [15]–[18].

In 2018, King Abdulaziz University launched a Molecular Imaging Company (I-ONE) established by the Jeddah Valley company. The facility is operated by the radiopharmaceutical division of ITEL Telecomunicazioni S.R.L. company in addition to local experts from Jeddah Valley. The I-ONE center is the only center in the western region of Saudi Arabia that can provide FDG used in the cancer diagnosis process. The center has a PET trace 880 cyclotron that operates in either a single or dual beam mode. The typical current of use is currently 60 μA, the maximum current that can be used in the dual beam configuration is 130 μA, and the proton beam energy is equal to 16.5 MeV. Although the cyclotron can produce ¹⁸F using two targets, only one target is currently used in daily production. The targets are shown

in Figure 1. The I-ONE center produces ^{18}F radioisotope ($T_{1/2} = 109.77$ min), which is used to produce the tracer ^{18}F fluorodeoxyglucose (^{18}F FDG), which can be used in the inhouse clinic or delivered to customers in close proximity to the center. It should be noted that the center objective is to expand and produce other radioactive materials that can be used outside the medical field for research and development [15].

The motivation of this work is to characterize the I-ONE PETtrace cyclotron. The Department of Nuclear Engineering at King Abdulaziz University is interested in the Neutron Activation Analysis (NAA) research area. The thermal neutron flux generated by medical cyclotrons is comparable with those generated by research reactors at $\sim 10^{6-8}$ n. cm^{-2} . Sec^{-1} . With a neutron source that can provide such an amount of thermal flux, the need for a neutron generator is greatly reduced [16]. There are some restrictions around using cyclotrons for NAA such as working around the production time of the cyclotron, and the high dose rate inside the cyclotron room following production. These challenges dictate the type and number of activated elements that can be researched using medical cyclotrons.

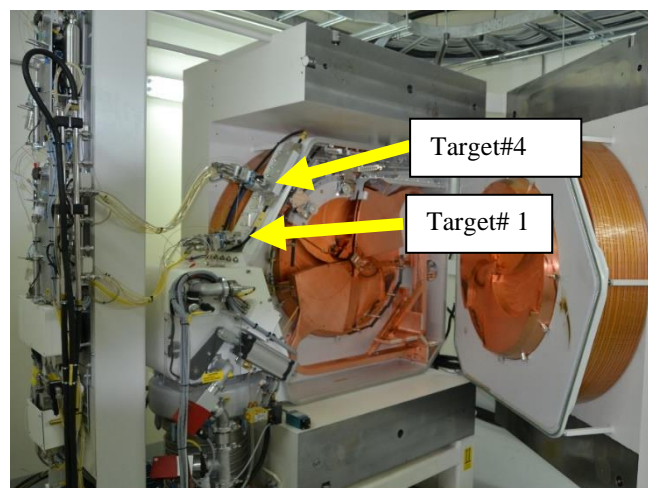


Figure 1: Demonstration of the I-ONE PET trace 880 cyclotron targets' locations.

2. Materials and Methods

2.1. Cyclotron room

The I-ONE cyclotron facility is divided into 3 rooms. These rooms, as shown in Figure 2, are the control room, power supply room, and cyclotron vault. The control room is where the operator sits and operates the cyclotron during production time. The power supply room contains many vital parts including the cooling system, electric power supply, power supply of the magnetic coil, radio frequency power generator

and control cabinets. Given the maze is constructed with multiple angles and dog legs, the neutron flux emitted from the cyclotron vault is substantially reduced. The vault was constructed using cement following the manufacturer’s recommendations. The length, width, and height of the vault are $4 \times 4 \times 5$ m, respectively and the thicknesses of the walls, ceiling, and floor are $2.5 \times 2.5 \times 3.5$ m, respectively. The design of the facility ensures that radiation protection principles are adhered to [17].

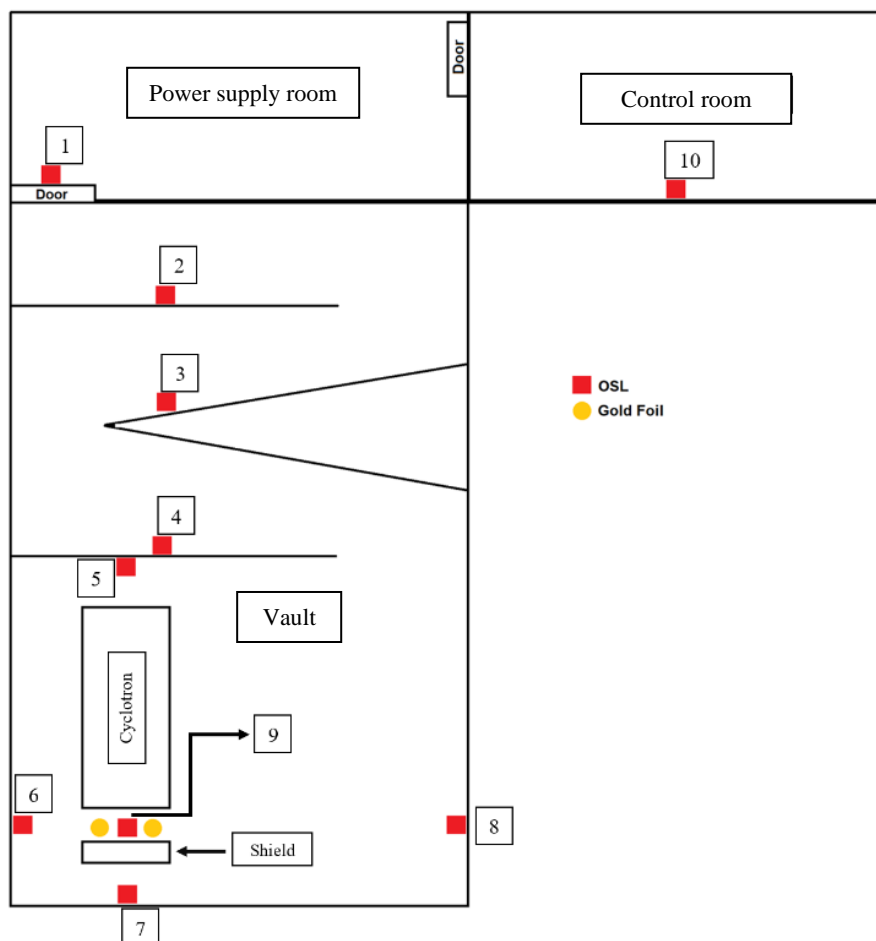


Figure 2: The I-ONE cyclotron facility layout including 3 rooms (control room, power supply room, and cyclotron vault). Also, the ten OSLs and gold foil’s position are illustrated.

2.2. Dose Estimation

The research team selected ten locations at 160 cm height from the ground to estimate the dose as illustrated in Figure 2. These locations are where staff may be exposed to the radiation during the ^{18}F production, maintenance, target refilling, and other production-related activities that require access to the cyclotron facility. The locations from 5 to 9 have higher radiation exposure due to scattering. Because of the maze design, the long-distance from the vault and the shielding, locations 4 to 1 and 10 have lower radiation exposure. Optically Stimulated Luminescence (OSL) detectors were used to measure the dose

at those positions. At the time of dose measurement, the cyclotron irradiation time and the beam current were 47 minutes and 60 μAm , respectively. The experiment was designed to carry out two measurements, one before production, which will estimate the background radiation, and the other one during the production of FDG. This setup ensures that both scenarios of low and high-level radiation are accounted for. In each measurement, the OSLs were exposed to the radiation for one day. The OSL cards were read directly after they were collected at the Center for Training and Radiation Prevention in the university campus.

2.3. Flux Estimation

Foil Activation technique is widely recognized as a method to estimate the neutron flux in a variety of applications, including the medical field [18]–[24]. In this experiment, a pure gold foil was utilized as a neutron monitor. The foil (Gold foil 0.004" 3n5) was purchased from EPSIMetals® as a sheet that has a length, width, and thickness of 5, 2.5, and 0.01 cm, respectively [25]. The goal behind fixing the holder at that location is to study the spatial neutron flux distribution around target# 1 shown previously in Figure 2. The researchers have a goal that is to design a 3D holder and base to minimize the variations in the measurements. The design of the 3D model allows for the examination of the neutron flux at eight elevations in multiple locations covering an area of 308 cm^2 . Figure 3 shows target#1, where a fixed sample holder was used to hold the gold disks in front of the target and the 3D printed holder with its projected location.

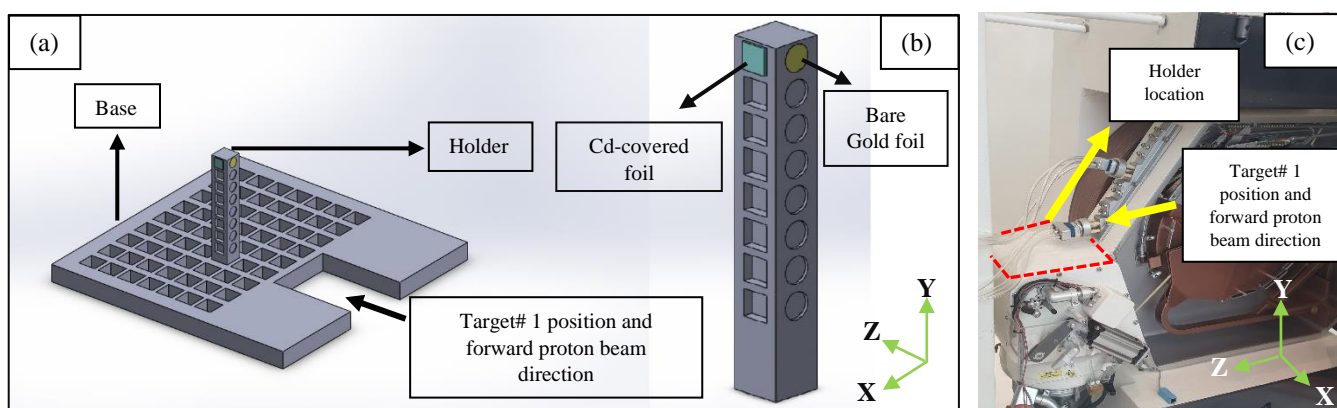


Figure 3: (a) The proposed design of the 3D holder and the base together with (b) the projected position of the bare gold (yellow color) and cadmium covered gold foil (cyan color), and (c) the location where the fixed holder was placed behind target #1, and where the 3D holder will be placed

The gold foil was shaped using a laser cutting machine to 1 cm diameter disks. The activated foil mass is 0.1551 grams. To calculate the epithermal flux, a 1x1 cm^2 cadmium sheet was used as a thermal neutron filter [26]. The cadmium sheet is folded on the bare gold foil allowing epithermal and fast neutrons to

traverse through it and the gold foil while filtering against the thermal neutrons. The measurements of both samples were carried out using a Canberra Broad Energy Germanium (BEGe) detector. Initially, the BEGe detector was calibrated for energy and efficiency using Cs-137, Co-60, and Ba-133 check sources. The efficiency curve was generated and then fitted to a 4th-degree polynomial function listed in equation 2, and the efficiency curve is shown in Figure .

$$Efficiency = e^{(a_0 \times (\ln(E))^{-1}) + (a_1 \times (\ln(E))^0) + (a_2 \times (\ln(E))^1) + (a_3 \times (\ln(E))^2)} \quad (2)$$

Where E is the energy at which the efficiency is calculated in keV, and a₀, a₁, a₂, a₃ are the fitting coefficients.

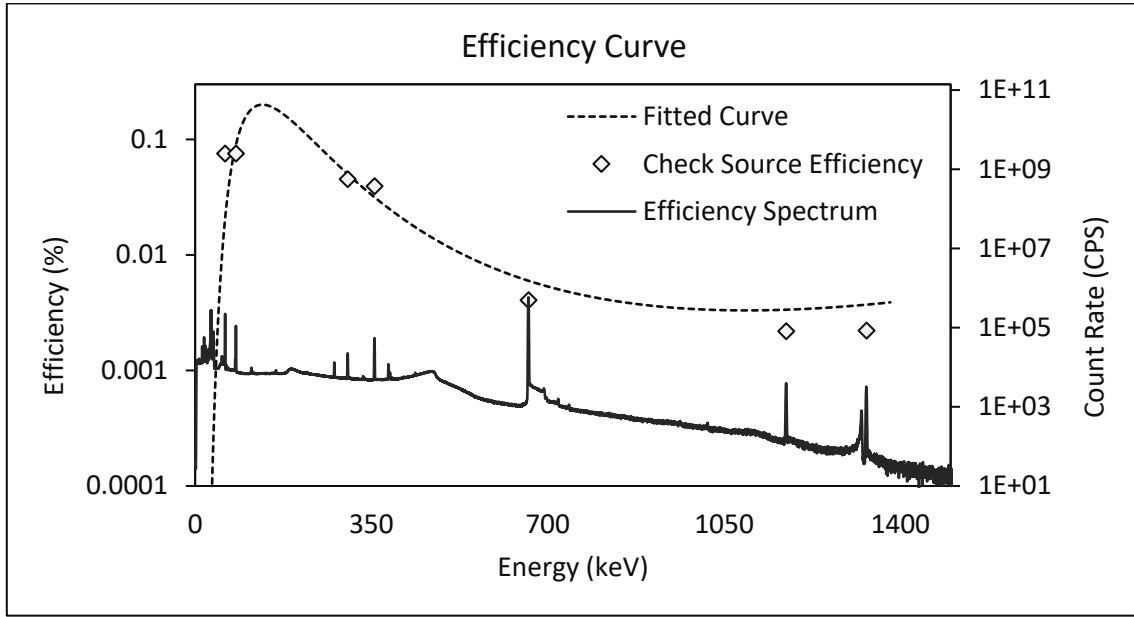


Figure 4: Generated efficiency curve using Cs-137, Co-60, Ba-133 check sources. The measured spectrum of the check sources is also exhibited

As a result of the activation, a gamma-ray with a 411.86 keV is emitted by the following reaction $^{197}\text{Au} (n, \gamma)^{198}\text{Au}$. The gold foil is measured for 5 consecutive days to obtain counting statistics of less than 1%. The efficiency and activity of the activated gold foil were calculated as well as the neutron flux.

2.4. Monte Carlo Simulation using GATE

GATE is an open-source Monte Carlo simulation toolkit that provides well-validated physics models that facilitate the simulation of medical physics and radiation protection applications [27]–[29].

The cyclotron component dimensions and other physical specifications were obtained from the cyclotron user manual. Other structures in the room, such as room dimensions and shield, were measured manually.

Since it would be difficult to simulate 60 μA of protons, the simulation was split into two stages. The first part starts with the emission of 2 billion protons that transverse several cyclotron components, such as the machine and target gold foils, before hitting the enriched water target inside a niobium key-hole shaped container. Neutrons and gamma-rays produced within the cyclotron structure are stored in a phase space file and then killed, concluding the first stage.

In the second stage, the proton source is replaced by gamma and neutron sources. Both sources derive their characteristics, such as energy distribution, momentum, and emission position, from the stored phase-space files. 500 million particles were used in this stage. The dose was calculated for positions 4-9 (see Figure 2) and the flux was measured in the same location as the gold foil. The fraction of particles penetrating the room walls are relatively low. Therefore, to calculate the dose with high statistical accuracy in positions 1, 2, 3, and 10, a very large number of particles is required. However, such a number of particles would increase the simulation time significantly and thus measuring the dose at these positions was avoided.

The dose measurement was carried out using the dose actor tool in GATE. The dose information was collected in water volumes having the same dimensions as the OSLs used in the experiments. It was not necessary to use OSL as a material as the dose measured experimentally is corrected to represent dose to water. The flux was measured using the energy spectrum actor. It should be noted that while the OSL cards were left in the cyclotron room for 24 hours, the dose collected in simulation only reflects the actual production time. All simulation results were rescaled to represent the doses and flux resulting from a 60 μA proton beam.

The physics package “QGSP_BIC_HP” was used as it provides high precision neutron models and accurate physics models for protons and gamma [30].

3. Results and Discussion

The differences between the dose measured before and after irradiation and those determined from simulation are highlighted in Table 1. Closer inspection of Table 1 shows that OSLs 1 to 3 and 10 after irradiation have measured dose rates less than 1 mSv/hour. Although the access to control room 2 is not permitted during irradiation, both control rooms have low dose rates compared to other locations in the

cyclotron room. The values of the dose rate increase significantly after irradiation. The measured dose after irradiation was divided by the irradiation time.

Table 1: OSL experimental and simulation dose measurements

OSL Number	Dose Rate ($\mu\text{Sv}/\text{hour}$)			
	Before Irradiation	After Irradiation	Simulation	Simulation Uncertainty
1	4.62	58.60	-	-
2	4.29	79.53	-	-
3	5.76	158.04	-	-
4	4.57	1.69 E+03	1.15E+04	13%
5	4.59	4.07 E+04	1.26E+05	4.5%
6	3.77	5.51 E+05	5.47E+05	2.0%
7	3.82	8.58 E+04	5.23E+05	2.2%
8	5.59	9.71 E+04	9.40E+04	5.2%
9	4.19	2.46 E+06	3.38E+06	0.9%
10	4.10	61.91	-	-

The data show OSL locations 1-4 and 10, which are the furthest from the cyclotron target, register the lowest dose after irradiation compared to the rest of the cards. On the other hand, OSL cards 5-9 close to the cyclotron vault register a sharp increase in dose rate. The OSL 7 and 8 dose rates, respectively, were 1 to 2 orders of magnitude less than OSL 6 and 9. This is due to the shielding in front of the target which reduces a significant amount of radiation to reach OSL 7, as well as the long-distance (around 2.5 m) between the target and OSL 8. Even though the level of doses increased when the irradiation process started, the dose rate inside the two control rooms (OSL 1 and 10) have acceptable and safe dose rates.

The simulated dose rate exhibited an acceptable agreement with the measured dose rate, as illustrated in Figure 3. The simulation was only performed for the vault setup, the whole irradiation facility was not considered in the simulation. Also, the cyclotron body's materials was not accounted for during the simulation. This approach was preferred to reduce simulation time. Subsequently, OSL 4, 5 (behind the body of the cyclotron) and 7 (behind the shield) measured dose values were less than the simulated values by an order of magnitude. OSLs 6, 8 and 9 had the same order of magnitude as the simulation and almost equal to measured dose values.

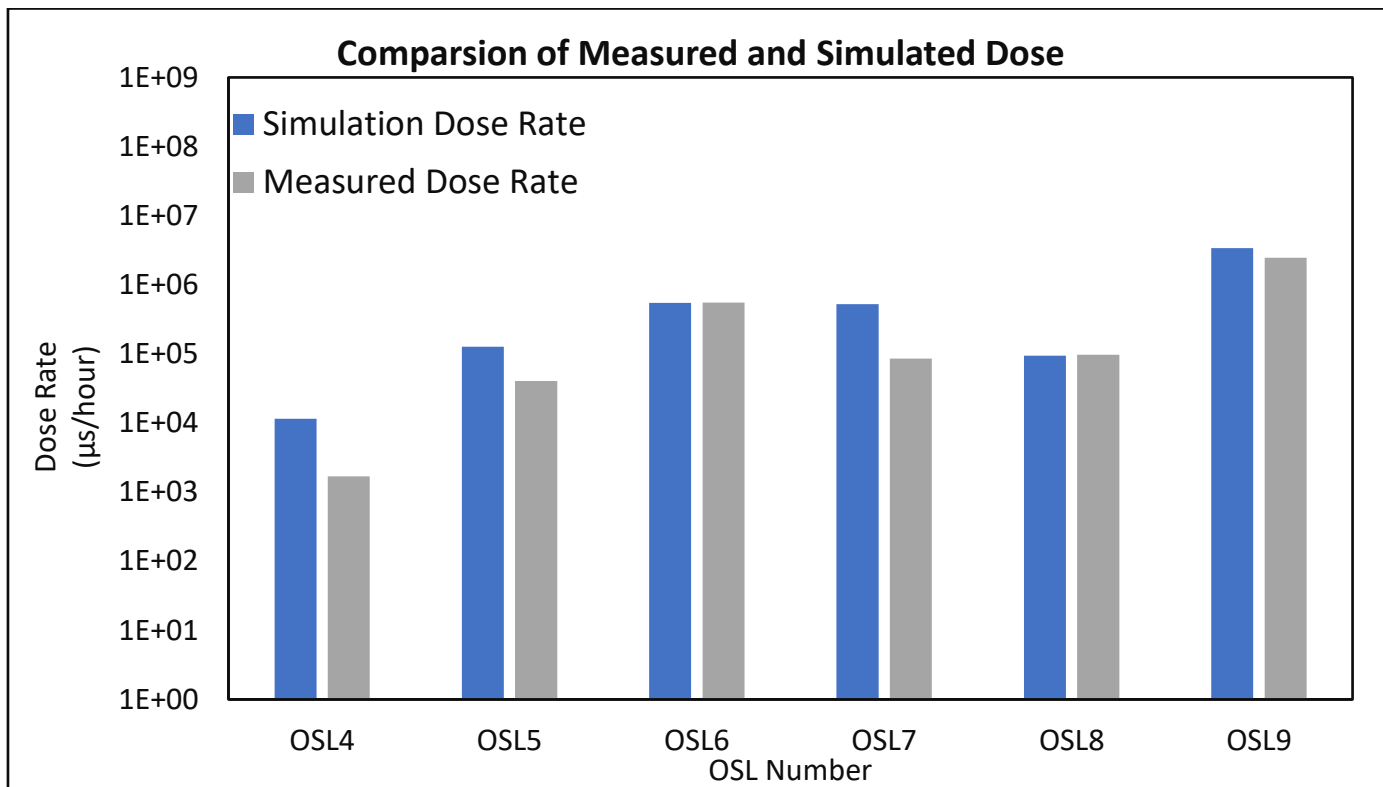


Figure 3: Dose rate trend inside the I-ONE irradiation facility for OSLs 4 to 9

In **Error! Reference source not found.** part (c), the bare gold foil was placed in a fixed holder at 20 cm in both z and y-axis from the target, which was recommended by the cyclotron manufacturer. The cyclotron facility was not characterized before; therefore, these distances were selected as a precautionary measure to avoid hindering the production process. At the same time, the 3D model should fully map the neutron flux around the target has started.

The bare gold foil was irradiated for 47 minutes and left at the vault for approximately 24 hours waiting for the radioactivity to decrease to a safe level to enter the vault. Due to the relatively long waiting time after irradiation, samples that undergo activation must have half-lives more than one day to attain acceptable counting results. The activated gold foil was counted using the Canberra BEGe detector at the Center for Training and Radiation Prevention. The efficiency of the detector is energy-dependent and

crucial in flux estimation. At an energy of 411.8 keV, the activated bare gold (^{198}Au) net area, efficiency, and activity were found to be 14.662 counts per second, 0.02%, and $2.0\text{E-}02 \pm 7.95\text{E-}04$ uCi, respectively. The fixed holder that held the gold foil is perpendicular to target#1. The neutron flux at that location was found to be $1.5\text{E+}06 \pm 5.94\text{E+}04$ neutrons. cm^{-2} . sec^{-1} . Also, the simulated results using the same set up showed an excellent agreement with a flux of $5.5\text{E+}06$ neutrons. cm^{-2} . sec^{-1} . Neutron and gamma spectra generated by the simulation are shown in Figure 4 and Figure 5. Table 2 compares thermal flux from this work to other studies carried out at other facilities.

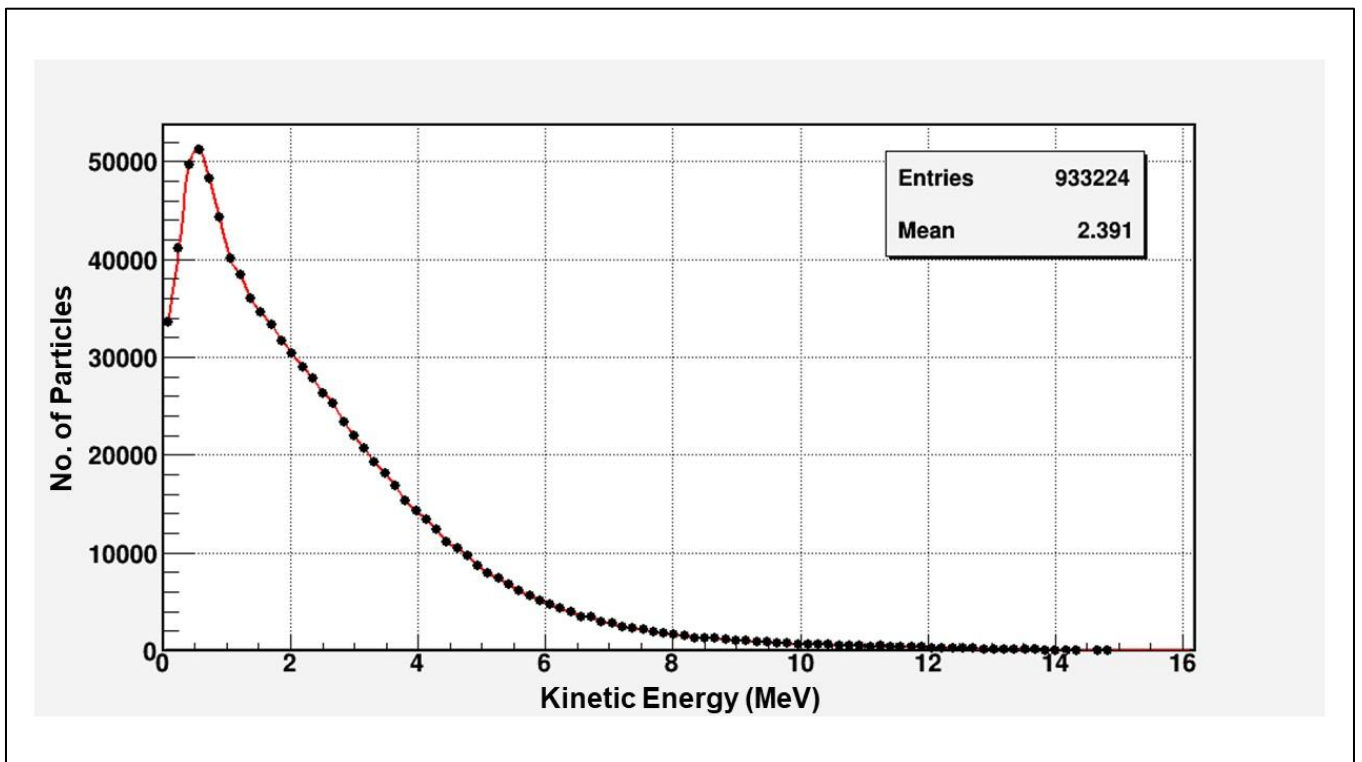


Figure 4: Simulated Neutron spectrum at the fixed sample holder where the gold foil is being activated

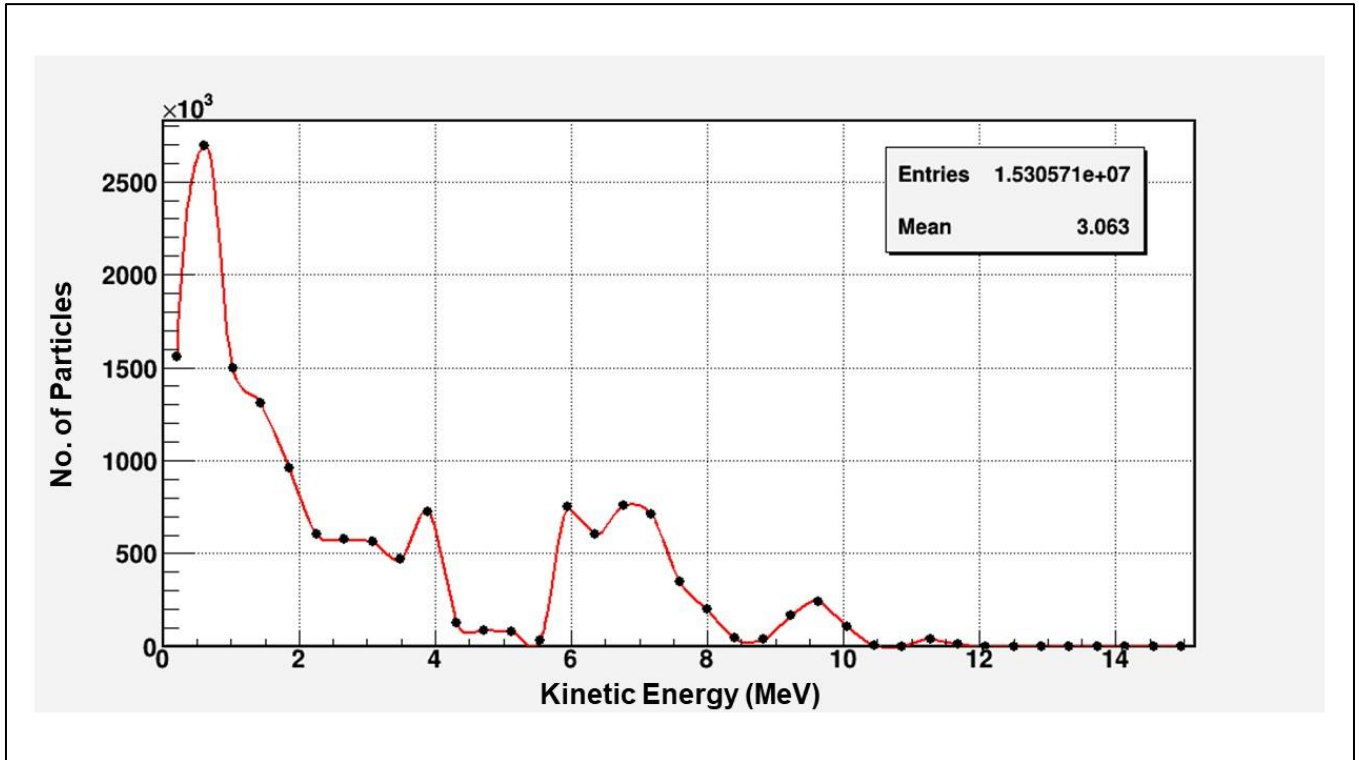


Figure 5: Simulated Gamma spectrum at the fixed sample holder where the gold foil is being activated

Table 2: Comparison between different cyclotron facilities [16]

	Type	Self-shield	Proton Energy (MeV)	Beam Current (uA)	Thermal Neutron Flux (n/cm ² .sec)	Neutron Dose Rate (μSv/h)
<u>This work</u>	PETtrace	x	16.5	60	1.5E+06	2.46 E+05
Toshioh et al.	PETtrace	Yes	16.5	40	1.00E+02	
Sakama et al.	HM-12S	Yes	12	35	<1.00E+2	
Hertel et al.	RDS	Yes	11	-	5.00E+01	
Lin et al.	RDS-111	Yes	11	80	7.70E+02	
Pant et al.	Eclipse	Yes	11	35	-	14.2
Ogata et al.	HM-18	x	18	20	10 ⁽⁵⁻⁶⁾	
Fujibuchi et al.	HM-18	x	18	20	10 ⁽⁵⁻⁶⁾	
Fernandez et al.	Cyclon	x	18	30	1.00E+07	
Mendez et al.	Cyclon	x	18	30	10 ⁽⁵⁻⁶⁾	
Sheu et al.	PETtrace	x	16.5	75	-	5.48E+05

4. Conclusion

The neutron flux behind target 1 of the PET trace 880 cyclotron at the I-ONE facility at King Abdulaziz University was measured using activated gold foils. The generated flux was measured to be $1.5\text{E}+06 \pm 5.94\text{E}+04$ neutrons. $\text{cm}^{-2} \cdot \text{sec}^{-1}$, which is the same order of magnitude listed by the cyclotron manufacturer. In addition to that, the flux was simulated using GATE Monte-Carlo simulation tool kit producing the same flux order of magnitude as the measurements. The distribution of flux behind targets 1, and 2 will be further studied to generate a map for the flux value and flux uniformity behind the targets so that the area behind the targets can be used as a thermal column for NAA research.

5. Acknowledgment

This project was funded by the Deanship of Scientific Research (DSR) at King Abdulaziz University, Jeddah, under grant no. RG-12-135-40. The authors, therefore, gratefully acknowledge DSR technical and financial support. In addition, the research team would like to thank the operating team at the I-ONE facility and the ITEL TELECOMUNICAZIONI SRL team for their continuous technical support to produce this work.

6. References

- [1] H. R. Vega-Carrillo, "Neutron energy spectra inside a PET cyclotron vault room," *Nucl. Instruments Methods Phys. Res. Sect. A Accel. Spectrometers, Detect. Assoc. Equip.*, vol. 463, no. 1–2, pp. 375–386, 2001, doi: 10.1016/S0168-9002(01)00234-0.
- [2] P. Schmor, "Review of cyclotrons for the production of radioactive isotopes for medical and industrial applications," *Rev. Accel. Sci. Technol. Accel. Appl. Ind. Environ.*, vol. 4, pp. 103–116, 2012, doi: 10.1142/S1793626811000574.
- [3] B. D. Jeffries *et al.*, "Characterization of the neutron flux during production of ^{18}F at a medical cyclotron and evaluation of the incidental neutron spectrum for neutron damage studies," *Appl. Radiat. Isot.*, vol. 154, no. May, 2019, doi: 10.1016/j.apradiso.2019.108892.
- [4] J. J. Martinez-Serrano and A. D. De Los Rios, "Predicting induced activity in the havar foils of the ^{18}F production targets of a PET cyclotron and derived radiological risk," *Health Phys.*, vol. 107, no. 2, pp. 103–110, 2014, doi: 10.1097/HP.0000000000000064.
- [5] A. Yamadera, "RESIDUAL LONG-LIVED RADIOACTIVITY DISTRIBUTION IN Year (from April to March)," pp. 621–631, 1994.
- [6] K. Masumoto, A. Toyoda, K. Eda, and T. Ishihara, "Measurement of the Spatial Distribution the Combination of Activation Kazuyoshi Masumoto , Akihiro of Neutrons in an Accelerator Room Detectors and an Imaging Plate Eda and Toyoyuki Ishihara by Toyoda , Kazuyoshi Radiation Science Center , High Energy Acc.," vol. 1, no. 1, pp. 12–16, 2002.
- [7] N. E. Hertel, M. P. Shannon, Z. L. Wang, M. P. Valenzano, W. Mengesha, and R. J. Crowe, "Neutron measurements in the vicinity of a self-shielded pet cyclotron," *Radiat. Prot. Dosimetry*, vol. 108, no. 3, pp. 255–261, 2004, doi: 10.1093/rpd/nch026.
- [8] R. Méndez, M. P. Iñiguez, J. M. Martí-Climent, I. Peñuelas, H. R. Vega-Carrillo, and R. Barquero, "Study of the neutron field in the vicinity of an unshielded PET cyclotron," *Phys. Med. Biol.*, vol. 50, no. 21, pp. 5141–5152, 2005, doi: 10.1088/0031-9155/50/21/013.
- [9] T. Fujibuchi *et al.*, "Measurement of thermal neutron fluence distribution with use of ^{23}Na radioactivation around a medical compact cyclotron," *Radiol. Phys. Technol.*, vol. 2, no. 2, pp. 159–165, 2009, doi: 10.1007/s12194-009-0060-7.
- [10] K. Masumoto *et al.*, "Effectiveness of self-shielding type cyclotrons," *Prog. Nucl. Sci. Technol.*, vol. 4, pp. 223–227, 2014, doi: 10.15669/pnst.4.223.
- [11] C. Birattari, M. Bonardi, A. Ferrari, and M. Silari, "Neutron activation of air by a biomedical cyclotron and an assessment of dose to neighbourhood populations," *Radiation Protection Dosimetry*, vol. 14, no. 4, pp. 311–319, 1986, doi: 10.1093/oxfordjournals.rpd.a079662.
- [12] G. Horitsugi *et al.*, "Radiologic assessment of a self-shield with boron-containing water for a compact medical cyclotron.," *Radiol. Phys. Technol.*, vol. 5, no. 2, pp. 129–137, 2012, doi: 10.1007/s12194-012-0147-4.
- [13] A. Infantino, L. Valtieri, G. Cicoria, D. Pancaldi, D. Mostacci, and M. Marengo, "Experimental measurement and Monte Carlo assessment of Argon-41 production in a PET cyclotron facility," *Phys. Medica*, vol. 31, no. 8, pp. 991–996, 2015, doi: 10.1016/j.ejmp.2015.07.146.

- [14] D. G. Jang, J. M. Kim, and J. H. Kim, "Design of the shielding wall of a cyclotron room and the activation interpretation using the Monte Carlo simulation," *J. Instrum.*, vol. 12, no. 1, 2017, doi: 10.1088/1748-0221/12/01/T01003.
- [15] "I-ONE." <http://www.ione.com.sa/> (accessed May 06, 2020).
- [16] T. Fujibuchi *et al.*, "Comparison of neutron fluxes in an 18-MeV unshielded cyclotron room and a 16.5-MeV self-shielded cyclotron room," *Radiol. Phys. Technol.*, vol. 5, no. 2, pp. 156–165, 2012, doi: 10.1007/s12194-012-0149-2.
- [17] G. Healthcare, "PETtrace 800 Series Site Planning Guide," 2013.
- [18] K. Kobayashi, S. Yamamoto, K. Itsuro, R. Miki, and T. Itoh, "Measurement of Neutron Flux Spectrum by," vol. 25, pp. 21–34, 1988.
- [19] W. S. Liu, S. P. Changlai, L. K. Pan, H. C. Tseng, and C. Y. Chen, "Thermal neutron fluence in a treatment room with a Varian linear accelerator at a medical university hospital," *Radiat. Phys. Chem.*, vol. 80, no. 9, pp. 917–922, 2011, doi: 10.1016/j.radphyschem.2011.03.022.
- [20] A. Konefał, M. Dybek, W. Zipper, W. Łobodziec, and K. Szczucka, "Thermal and epithermal neutrons in the vicinity of the Primus Siemens biomedical accelerator," *Nukleonika*, vol. 50, no. 2, pp. 73–81, 2005.
- [21] A. Konefał, A. Orlef, M. Dybek, Z. Maniakowski, K. Polaczek-Grelik, and W. Zipper, "Correlation between radioactivity induced inside the treatment room and the undesirable thermal/resonance neutron radiation produced by linac," *Phys. Medica*, vol. 24, no. 4, pp. 212–218, 2008, doi: 10.1016/j.ejmp.2008.01.014.
- [22] A. Konefał, A. Orlef, M. Łaciak, A. Ciba, and M. Szewczuk, "Thermal and resonance neutrons generated by various electron and X-ray therapeutic beams from medical linacs installed in polish oncological centers," *Reports Pract. Oncol. Radiother.*, vol. 17, no. 6, pp. 339–346, 2012, doi: 10.1016/j.rpor.2012.06.004.
- [23] F. Nobuhara, M. Kuroyanagi, K. Masumoto, H. Nakamura, A. Toyoda, and K. Takahashi, "Neutron transport calculation for Activation Evaluation for Decommissioning of PET cyclotron Facility," *EPJ Web Conf.*, vol. 153, 2017, doi: 10.1051/epjconf/201715304007.
- [24] K. Haddad, O. Anjak, and B. Yousef, "Neutron and high energy photon fluence estimation in CLINAC using gold activation foils," *Reports Pract. Oncol. Radiother.*, vol. 24, no. 1, pp. 41–46, 2019, doi: 10.1016/j.rpor.2018.08.009.
- [25] "ESPI Metals." <https://espi Metals.com/index.php/component/content/article/355-online-catalog/gold-au/364-gold-au?Itemid=135> (accessed May 08, 2020).
- [26] B. Abdullahi and M. T. Tsepav, "The Utilization of Cadmium as Thermal Neutron Filter in the Characterization of Gold Matrix in NIRR-1," vol. 2, no. 5, pp. 281–285, 2012, [Online]. Available: <http://www.ejournalofsciences.org>.
- [27] D. Sarrut *et al.*, "A review of the use and potential of the GATE Monte Carlo simulation code for radiation therapy and dosimetry applications," *Med. Phys.*, vol. 41, no. 6Part1, p. 064301, May 2014, doi: 10.1118/1.4871617.
- [28] S. Jan *et al.*, "GATE V6: a major enhancement of the GATE simulation platform enabling modelling of CT and radiotherapy," *Phys. Med. Biol.*, vol. 56, no. 4, pp. 881–901, Feb. 2011, doi: 10.1088/0031-

9155/56/4/001.

- [29] S. Jan *et al.*, “GATE: A simulation toolkit for PET and SPECT,” *Phys. Med. Biol.*, vol. 49, no. 19, pp. 4543–4561, Oct. 2004, doi: 10.1088/0031-9155/49/19/007.
- [30] Geant4 Collaboration, “Physics Reference Manual,” 2018.